CrossMark

Analysis of In-Room mm-Wave Propagation: Directional Channel Measurements and Ray Tracing Simulations

F. Fuschini[1] · S. Häfner[2] · M. Zoli[1] · R. Müller[2] ·
E. M. Vitucci[1] (ORCID) · D. Dupleich[2] · M. Barbiroli[1] ·
J. Luo[3] · E. Schulz[3] · V. Degli-Esposti[1] · R. S. Thomä[2]

Abstract Frequency bands above 6 GHz are being considered for future 5G wireless systems because of the larger bandwidth availability and of the smaller wavelength, which can ease the implementation of high-throughput massive MIMO schemes. However, great challenges are around the corner at each implementation level, including the achievement of a thorough multi-dimensional characterization of the mm-wave radio channel, which represents the base for the realization of reliable and high-performance radio interfaces and system architectures. The main properties of the indoor radio channel at 70 GHz, including angular and temporal dispersion as well as an assessment of the major interaction mechanisms, are investigated in this study by means of UWB directional measurements and ray tracing simulations in a reference, small-indoor office environment.

✉ E. M. Vitucci
enricomaria.vitucci@unibo.it

F. Fuschini
franco.fuschini@unibo.it

S. Häfner
Stephan.Haefner@tu-ilmenau.de

M. Zoli
marco.zoli5@unibo.it

R. Müller
mueller.robert@tu-ilmenau.de

D. Dupleich
Diego.Dupleich@tu-ilmenau.de

M. Barbiroli
marina.barbiroli@unibo.it

J. Luo
Jianluo@huawei.com

1 Introduction

The apparently endless increase of bandwidth-hungry applications, together with the worldwide diffusion of wireless devices like smartphones and tablets is fostering an extended and effective usage of the radio spectrum.

Feverish activities aiming at improving the exploitation of the most congested frequency bandwidths have been already carried out and are still going on, including the bandwidth reallocation from broadcast to personal communications triggered by the analog TV switch-off, or new regulatory approaches aiming at a better spectrum management such as licensed shared access. At the same time, underutilized frequency bands in the millimeter wave spectrum (30–300 GHz) have gained increasing attention and now appear as the most likely candidates to host the forthcoming multi-gigabit, 5G wireless applications. In this regard, investigations on the development of International Mobile Telecommunication services in the frequency range between 24.25 and 86 GHz have been claimed during the 2015 World Radiocommunication Conference [1].

While the perspective is rather promising, the development of mm-wave technologies and network planning strategies is nevertheless at an early stage, since many aspects must be still discussed and fully understood. Radio channel modeling represents one of the open issues, since the vast propagation studies on the directional and wideband channel characteristics of the recent past have mainly addressed frequency bands up to 6 GHz.

In order to bridge this gap, investigations on radio channel properties at mm-waves have become a focus of the past few years. Recent studies span from indoor scenarios [2], where the IEEE 802.11ad standard [3] finds commercial applications [4], to outdoor environments, where mm-waves are being considered for both end-user radio access [5] and wireless backhauling [6].

Due to the tiny wavelength, mm-wave wireless systems are expected to house large antenna arrays, especially at the base station end, thus enabling the implementation of spatial diversity, beamforming (BF) and spatial multiplexing [7, 8] MIMO schemes. The effectiveness of such techniques depends on the multidimensional and wideband properties of the channel (e.g.,

E. Schulz
egon.schulz@huawei.com

V. Degli-Esposti
v.degliesposti@unibo.it

R. S. Thomä
reiner.thomae@tu-ilmenau.de

[1]   Department of Electrical, Electronic and Information Engineering, "G. Marconi" (DEI), University of Bologna, IT-40136 Bologna, Italy

[2]   Ilmenau University of Technology, 98684 Ilmenau, Germany

[3]   European Research Center, Huawei Technologies Düsseldorf GmbH, 80992 Munich, Germany

space/time dispersion, multipath correlation properties), and therefore the design of wireless systems operating in the mm-wave band will benefit from a thorough multipath propagation characterization. This is usually achieved through measurement campaigns [9, 10] or exploiting ray tracing (RT) prediction models [11–14], which can in principle simulate the multipath channel. It is worth noticing that the computation capabilities provided by today's multicore processors and graphical processing units (GP-GPUs) can cope with the computational burden required by RT simulations, thus partly removing the bottleneck that used to limit the massive use of RT models [15].

In this work, in-room wireless propagation at 70 GHz is investigated by means of directional channel measurements using RT simulations as both an analysis tool and a reference propagation model to be assessed and calibrated. The work represents the continuation and the completion of the preliminary investigation carried out in [10], but here the relatively unexplored 70 GHz band is considered instead of the 60 GHz one, the measurement set up is more advanced and the overall scope of the work is wider and more complete. The work has three main purposes: (1) identifying the dominant electromagnetic interaction mechanisms (reflection, diffraction, transmission, scattering) and the characteristics of the resulting angular and temporal spreading of the channel; (2) investigating the impact of the environmental clutter (i.e., indoor furnishings) on propagation as well as the actual need for an item-level description of the scenario to get satisfactory RT prediction; and (3) corroborating the reliability of a ray based approach to channel modeling at mm frequencies.

With reference to the first issue, special attention has been devoted to the role played by diffuse scattering. Many studies have shown that scattering effects may be important at sub-6-GHz frequencies [11, 16, 17], because of the presence of many objects generating non-specular, scattered contributions due to their size being comparable to the wavelength, to surface unevenness or to volume dishomogeneities [18]. Whether diffuse scattering becomes stronger or—on the contrary—weaker at mm-wave with respect to lower frequencies is still under debate [19], and even conflicting analyses can be found in the literature. For instance, according to [9], the mm-wave radio channel seems dominated by specular interactions, with negligible scattering effects, and in [20] at least 80% of the received power at 60–70 GHz is shown to be carried by specular contributions. At the same time, a full-scattering model has been proposed for mm-wave channel modeling [21], and backscattering from a brick wall has been estimated in [18] slightly stronger at mm-wave than at lower frequencies. These apparently conflicting conclusions represent a motivation for this work and more generally for further investigation on the topic.

The remaining part of the paper is organized as follows: Section 2 outlines the experimental setup used for the study, while Section 3 describes the RT simulation software. Section 4 shows the major results of the work, whereas Section 5 shortly investigates the sensitivity of RT predictions to the accuracy in the environment description. Final considerations are outlined in Section 6.

2 Measurement Setup

Mm-wave measurements have been carried out in a small office located at the Technische Universität Ilmenau during daytime with no people around [22–24].

The room, which has a size of nearly 20 m^2, is representative of most small-office environments and contains usual indoor furnishing objects like wooden desks, cabinets, a

PC, etc. as sketched in Fig. 1 and partly shown in Fig. 2. Lateral and ceiling walls are made of slightly rough concrete, whereas the floor consists of a thin carpet on the gross concrete of the ground. Two thick windows surrounded by a wide metallic frame and a large heat radiator are present on the upper wall in Fig. 1, whereas a heavy metallic door (kept close during the measurements) and a thin metallic blackboard are placed on the opposite wall.

The measurement system is an ultra-wideband (UWB) 70-GHz Channel Sounder (CS) designed by TU Ilmenau, able to provide directional channel impulse responses (CIRs), as described in [18, 24]. It is based on an UWB M-Sequence chip-set and offers a 3-dB instantaneous bandwidth of 4 GHz after calibration, providing high resolution in time domain.

The setup involves different transmitter (TX) and receiver (RX) positions as shown in Fig. 1. The TX antenna is always 2.45 m high, mounted on a stable plate on a 3D positioner. In order to mechanically emulate a smart in-room access point, TXs can sweep both the elevation (El) and the azimuth (Az) plane in 15° steps, obtaining 13×13 spatial samples for TX2 and 13×7 spatial samples for TX1, respectively.

As shown by Fig. 3, the RX equipment is lightweight and mobile. In order to emulate different user positions, it has been moved over 7 positions inside the room (Fig. 1). The RX antenna is 0.9 m high over the ground and capable to scan only the azimuthal range from 0° to 360° in 15° steps at 0° elevation, corresponding to 24 different orientations. For every measurement position, the CS chain has been de-embedded in the frequency domain using back-to-back calibration and noise has been removed in the time domain using a threshold algorithm.
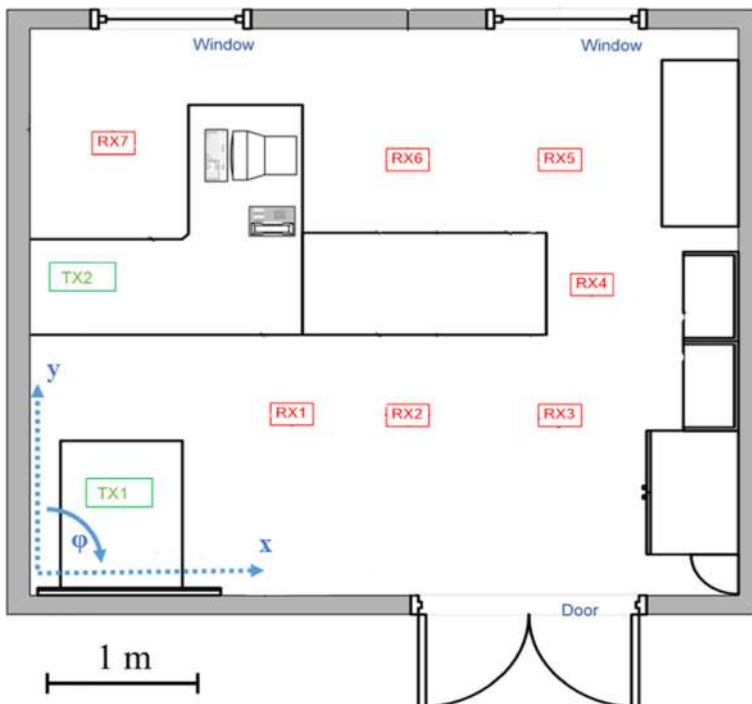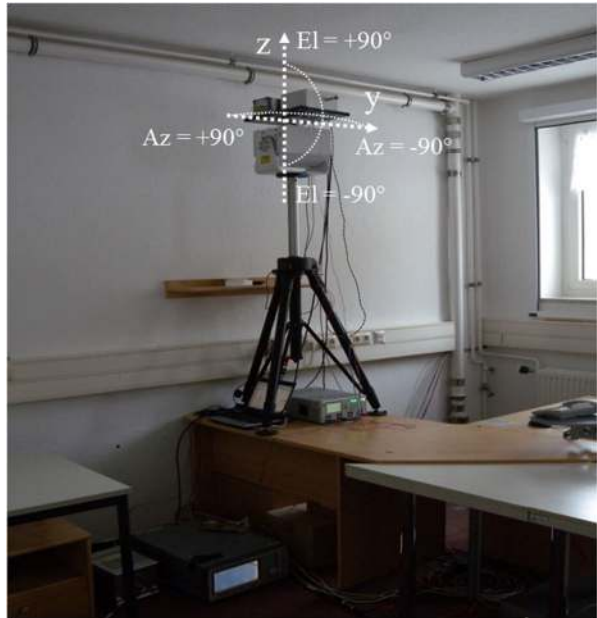

Fig. 1 2D map of the indoor office. TXs in *green* and RXs in *red*. Some details in *blue*

Fig. 2 TX2 mounted on the rotational positioner. Angular coordinates are overlaid in *white*

Owing to these properties, the measurement setup is representative of future mm-wave wireless system configurations, where the access-point is equipped with a large beamforming array, while the receiver can sport either an omnidirectional antenna if no pointing technique is implemented, or a directive beamforming antenna with a relatively limited pointing capability. To simulate occasional obstructions of the Line of Sight (LOS), non-LOS (NLOS) configurations have been realized in a couple of cases (TX1-RX7, TX2-RX4) through the introduction of an absorbing screen properly placed on the tables and close enough to the RXs to prevent the LOS.

Cylindrical dual-polarized horn antennas have been used at both the link ends, having a gain of 20 dBi and a half power beam width (HPBW) of about 15°, i.e., equal to the rotational step of the positioners, in order to limit the contribution of the same multipath components to different angular samples.

Fig. 3 RX mounted on the rotational positioner at position 2 in the office. Angular coordinates are overlaid in *white*

3 Ray Tracing Simulation

Software simulations in the measurements environment have been carried out with a 3D Ray Tracing (RT) tool specifically conceived for indoor environments and described with more details in [11]. In addition to the coherent interaction mechanisms modeled by geometrical optics (GO) and uniform theory of diffraction (UTD), i.e., specular reflection (simply labeled as "R" in the following), transmission ("T") and diffraction ("D"), diffuse scattering ("S") is also taken into account using the effective roughness (ER) model [11, 25]. The ER model can be easily embedded into ray based prediction tools in order to approximately but effectively account for non-specular contributions generated by surface roughness, surface unevenness (e.g., protruding elements) and/or volume dishomogeneities (e.g., buried cables and pipes), often not included into the input databases to limit their size or because simply unknown. The main parameter of the ER model is the scattering parameter S, which can generally assume different values in the backward (S_R) and forward (S_T) half spaces [26]. In particular, S_R^2 (S_T^2) corresponds to the percentage of power scattered in all the directions at the expense of reflection (transmission), while the intensity of reflected rays is accordingly reduced by a factor $1-S_R^2$ ($1-S_T^2$), to satisfy the power balance and ensure the physical soundness of the model. A directional scattering diagram centered around the directions of reflection (transmission) is often assumed, according to a second parameter α_R (α_T) inversely proportional to the width of the scattering lobes [18, 26].

While coherent interactions are tracked through a recursive, image-RT technique, diffuse scattering is implemented according to a ray launching (RL) approach, i.e., based on rays launched from the TX with a discrete angle step [11].

The setting of the main RT parameters is sketched in Table 1, corresponding to an effective trade-off between computational effort and prediction accuracy.

The RT geometrical input database consists of a vectorial 3D representation of the small office including the building frame (walls, ceiling and floor) and openings (door and windows—metallic frame included), the visible elements of the hydraulic and electric installations (heat radiator, ceiling lamps, external pipes and ducts), and the largest furnishings objects (tables, cabinets). The electromagnetic (em) parameters of the items constituting materials are also taken into account, as summarized in Table 2. The values reported in the table are gathered from the current literature for mm-wave bands, in order to check if satisfactory predictions can be achieved even without em parameters tuned to the specific scenario. For the sake of simplicity, the same scattering pattern is assumed for all objects, with both α_R and α_T equal to 5.

Table 1 Main RT simulation parameters		
	Maximum number of interactions for each ray	6
	Maximum number of reflections (R) for each ray	4
	Maximum number of diffractions (D) for each ray	1
	Maximum number of transmissions (T) for each ray	6
	Combined reflection and diffraction (RD)	Included
	Combined scattering and reflection (RS)	Included
	Angular step for ray launching of scattering rays (elevation and azimuth)	5°

Table 2 Em material parameters for RT simulation at 70 GHz (numbers within square brackets refer to the reference list)

Item	ε_R Value [Ref.]	σ Value [Ref.]	S_R Value [Ref.]	S_T Value [Ref.]
Wall	4.4 [27, 28]	1.0 [27, 29]	0.5 [18, 30]	0
Ceiling	4.4 [27, 28]	1.0 [27, 29]	0.5 [18, 30]	0
Floor	4.4 [27, 28]	1.0 [27, 29]	0.7	0
Table	2.8 [18, 29]	0.15 [18]	0.2 [18, 30]	0.3 [18]
Closet	2.8 [18, 29]	0.15 [18]	0.2 [18, 30]	0.3 [18]
Window	6.25 [29]	0.7 [29, 31]	0	0
Cable Duct	2.25 [31]	0 [31]	0.2	0.2
PC Monitor	10 [18]	0.8 [18]	0.8 [18]	0.8 [18]
Ceiling Lamp	2.0	1e8	0.7	0

4 Analysis of Results

In this section, CS measurements are analyzed and compared with RT simulations to determine radio channel characteristics and RT performance.

RT predictions are known to be sensitive to the accuracy in the description of both the scenario and the radiating elements. In the present work material characteristics (complex permittivity) have been derived from the literature, whereas the geometrical description of the environment has been derived "manually" through visual inspection and on-site measurement. The accuracy of RT simulation may therefore be limited by environment description errors, which could be reduced through advanced characterization techniques such as em measurement on the specific materials, and laser scanning techniques to acquire the environment geometry.

With reference to the antennas, a full 3D representation of the radiation patterns is embedded into the RT simulator.

4.1 Narrowband Analysis

For both RT simulations and measurements, the received power for each RX positions has been computed by adding up power contributions received from all TX and RX antenna orientations. At the RX side, this corresponds to representing the antenna as an omnidirectional antenna in the horizontal plane.

The comparison between measured and RT-predicted power is shown in Fig. 4 for both transmitter positions and confirms a good agreement for all RX positions, with a root mean squared error (RMSE) equal to 2.8 dB and to 0.7 dB for TX1 and Tx2, respectively.

The power contribution from the LOS path only (Friis Formula) is far below the actual received power, especially in RX positions closer to the TXs, where the LOS path has a high-elevation angle and is thus attenuated by the low gain of the RX antenna for that direction. Only including room multipath the agreement is satisfactory: this confirms that multipath plays a crucial role even in LOS conditions for the chosen setup, thus justifying the analysis carried out in the following sections.

The RT narrowband prediction capability has been checked against measurements also in NLOS conditions, with an overall accuracy in essential agreement with the LOS cases (prediction error equal to 2 dB and 3 dB for TX1-RX7 and TX2-RX4, respectively).
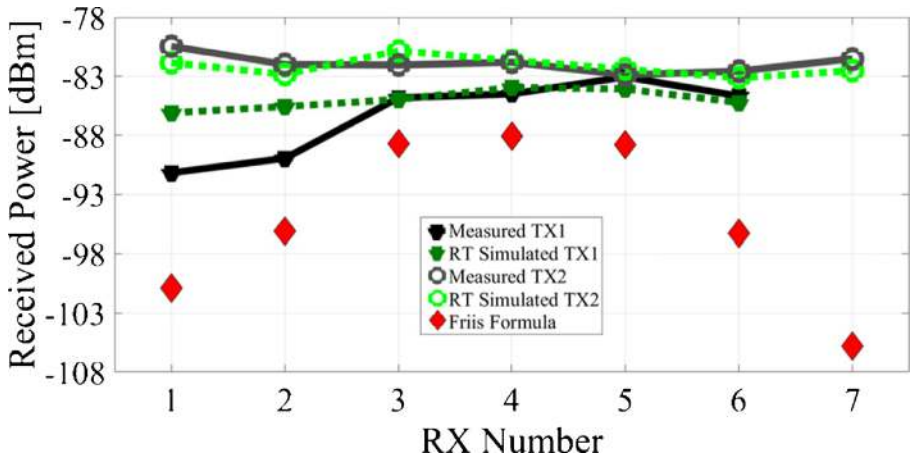
Fig. 4 Comparison between measurements and different models prediction for the LOS situations related to the TX2 case

4.2 Angular Dispersion

BF represents a key asset for millimeter wave systems to cope with the high propagation losses [7]. Generally speaking, BF performance depends on the multipath spatial properties: the larger the number of strong paths with spatially distinct direction of departure/arrival, the greater potential BF performance. This is especially true for multi-user BF schemes, where the presence of multiple, effective beam steering options can help reduce the interference between different users.

In order to investigate multipath spatial properties, power angle profiles (PAP) have been derived at the TX side, exploiting the wide angle of departure range both in elevation (−90°÷ + 90°) and azimuth (0°÷90° for TX1, −90°÷90° for TX2). An example of the (normalized) measured and simulated PAPs are respectively shown in Figs. 5 and 6 for the TX2-RX4 pair. The simulated PAP without diffuse scattering is also reported in Fig. 7 for reference.

The power value within each pixel is computed by integrating every directional CIR (i.e., for given TX/RX pointing directions) and then summing up the 24 spatial power samples
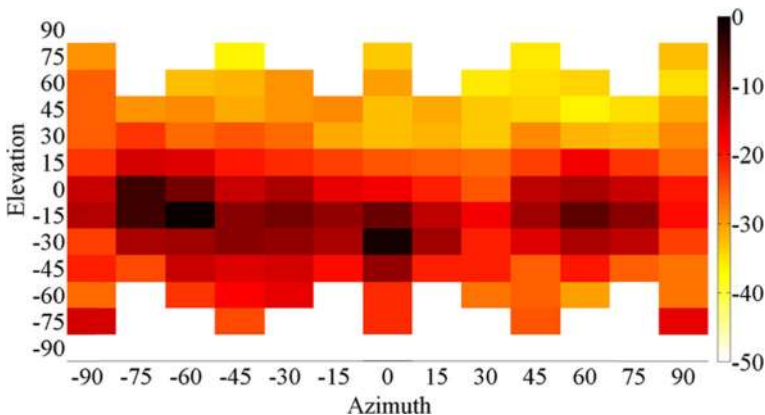

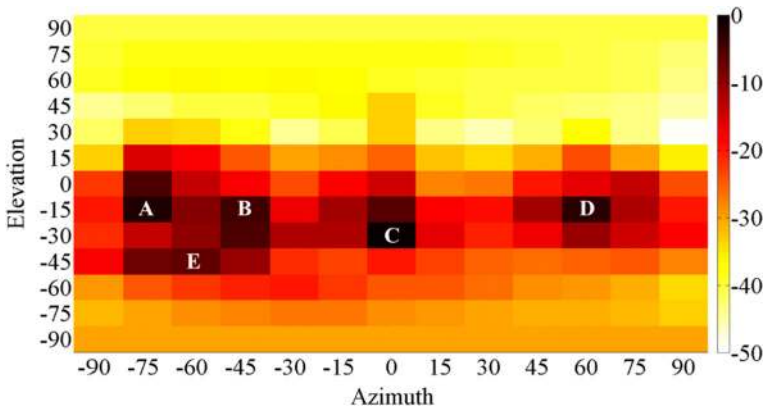Fig. 5 Measured PAP (TX2-RX4, LOS) in dB units

Fig. 6 RT simulated PAP (TX2-RX4, LOS) in dB units; strongest clusters highlighted with labels (**A–E**), see also Table 3

corresponding to the different pointings of the RX antenna. This analysis therefore refers to a TX-only beamforming scheme with an omnidirectional RX antenna.

The measured PAP is quite well reproduced by the RT tool for elevations limited to the range (−60°, 15°), whereas a general underestimation of about 10 dB is present when the TX antenna is pointing towards the ceiling or the floor. This disagreement for large elevation is a common trend for all the TX-RX pairs and may be attributed to several reasons:

(i)   the possible presence of unknown, metallic layers/grids underneath the ceiling/floor surface, which may affect back-scattering from those surfaces [32];

(ii) inaccuracies in the description of antenna radiation pattern, especially secondary lobes which can determine received power when the TX antenna is pointing away from the RX location;

(iii) scattering coefficients not optimized for the considered scenario, that can degrade prediction accuracy for large elevation angles, when diffuse scattering appears important, as evident comparing Fig. 7 with Fig. 6.
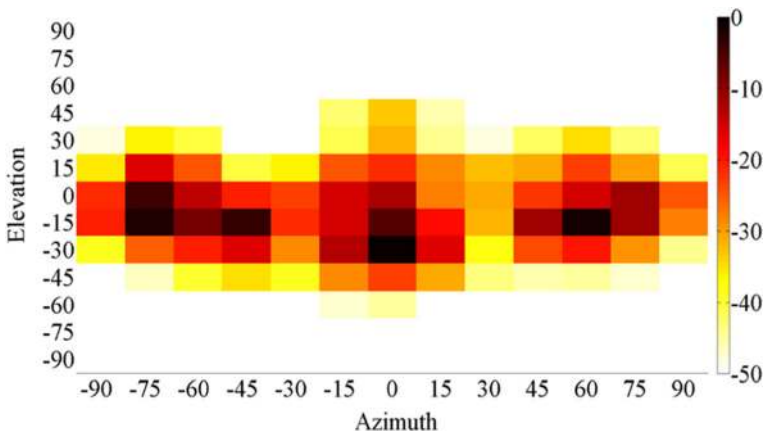

Fig. 7 RT simulated PAP (TX2-RX4, LOS) in dB units without scattering

The most important clusters marked as A–E in Fig. 6 are better analyzed in Table 3, using RT as a tool to identify the major propagation mechanisms generating each cluster. In agreement with [9, 20], reflection represents the dominant propagation contribution besides the LOS one (see sub-section E for a more extensive assessment). At the same time, diffuse scattering does not seem to be negligible as simulation without diffuse scattering (Fig. 7) yields a much more empty pattern, especially outside the elevation range (−60°, 15°), and without the "halo" around the major specular contributions. This is true for all RX positions, suggesting that diffuse scattering is a minor but non negligible mechanism, especially with regards to spatial channel spreading.

Furthermore, the cluster analysis in Table 3 also suggests that the strongest multipath contributions (clusters A, B, D) are fundamentally produced by interactions of the radiated wave with the "macro-structure" of the office, consisting of the building carrying structure (walls, floor and ceiling) and the openings on the walls (windows, door). To a lesser extent, smaller items may also determine still powerful replicas of the transmitted signal, especially if they are made of metal (e.g., cluster E—windows frame, heat radiator).

The overall PAP prediction accuracy of RT is assessed in Tables 4 and 5 using the root mean square error (RMSE), and the weighted RMSE (WRMSE, see following paragraph) computed for each available PAP and averaged over all RX locations.

Of course, predicting the signal angular distribution is much more difficult than predicting the overall received power, hence the higher RMSE values in Tables 4 and 5 as compared to the errors of Fig. 4.

It is evident that the errors are much smaller when ER diffuse scattering is taken into account. This may appear in contrast with previous considerations on scattering as a minor contribution.

This is due to the independence between RMSE and the intensity of the PAP for each angle of departure. Otherwise said, two equal errors affecting a strong and a weak contribution impact on the RMSE exactly in the same way. Therefore, the RMSE has been also computed by weighting each error with a coefficient equal to the relative power of the corresponding pixel, similarly to what happens with the propagation delays for the evaluation of the RMS delay spread (DS). The weighted RMSE (WRMSE in Tables 4 and 5) probably represents a more meaningful performance metric. In fact, the WRMSE values slightly increase if scattering is excluded from the RT simulations, the small change reflecting the relatively modest power contribution of scattering compared to specular contributions.

4.3 Temporal Dispersion

Temporal dispersion is a further, crucial issue to be considered for the design of the forthcoming multi-gigabit wireless networks, since frequency selectivity may in principle arise also for small delay spread values when large data rates must be supported.

Table 3 Analysis of the main detected cluster

Cluster	Az	El	Mechanisms	Objects
A	−75°	−15°	Multiple reflection	Walls/windows
B	−45°	−15°	Single reflection	Walls/windows
C	0°	−30°	Direct LOS	–
D	60°	−15°	Single/double reflections	Walls/windows/door
E	−45°	−45°	Scattered rays	Windows frames/cable ducts/radiator

Table 4 PAP errors TX1

TX1	RMSE		WRMSE	
RXs	With scat.	Without scat.	With scat.	Without scat.
1	12.9	21.7	4.6	5.7
2	11.3	22.2	4.4	6.5
3	7.2	19.0	2.1	5.4
4	8.4	21.4	2.5	3.9
5	10.8	22.3	4.1	5.0
6	8.7	18.3	2.5	3.4
7 NLOS	13.0	22.2	4.8	6.3
Average	10.3	21.0	3.6	5.2

In order to reduce the impact of the antennas radiation properties on the DS values, power delay profiles (PDPs) related to isotropic/omnidirectional patterns have been extracted from the available directional measurements. That is, an overall PDP has been derived for each TX-RX pair properly combining the CIR corresponding to the different antenna pointings, and the DS values have been then computed (Tables 6 and 7 for TX1 and TX2, respectively).

Tables 6 and 7 clearly show that scattering contributes to reduce the in-room delay spread. This result apparently conflicts with what found in previous studies carried out at lower frequencies in outdoor scenarios [33–35], but it can be explained by the different role played by the scattering phenomenon in the different environments.

Diffuse scattering can dramatically increase the number of propagation paths due to the greater divergence of the wavefront with respect to reflection and diffraction. For the same reason however, scattered paths are generally weaker. Multiple-bounce scattered rays are therefore usually negligible in practice, whereas single scattered ones can be important or not depending on the propagation conditions. In outdoor scenarios far objects (i.e., buildings) with direct visibility to both the TX and the RX are often present, and a single scattering interaction may produce significant long-delayed echoes, thus increasing the DS value [34].

In contrast, far scatterers cannot be present in a single room, where large delays (long traveled paths) must always correspond to a proportional number of undergone interactions. Therefore, single scattered contributions always have quite short delays, thus meaning that in room scattering effects can mainly affect the "head" of the PDP, corresponding to a (limited)

Table 5 PAP errors TX2

TX2	RMSE		WRMSE	
RXs	With scat.	Without scat.	With scat.	Without scat.
1	10.2	21.1	3.1	6.3
2	10.0	22.0	3.0	5.1
3	8.9	23.1	2.2	4.2
4 LOS	8.0	22.7	3.1	6.7
4 NLOS	7.9	22.6	2.0	4.1
5	8.1	22.3	1.9	3.5
6	10.5	23.4	3.2	5.7
7	9.7	20.3	3.1	5.6
Average	9.2	22.2	2.7	5.2

Table 6 DS errors TX1

TX1	Meas. DS (nsec.)	Predicted DS (nsec.)		Relative DS Error %	
RXs		With scat.	Without scat.	With scat.	Without scat.
1	8.1	7.7	8.2	−5	+1
2	8.8	8.4	7.6	−5	−14
3	9.4	10.7	11.0	+14	+17
4	9.1	10.3	10.7	+13	+18
5	9.1	11.0	11.5	+21	+27
6	9.2	10.4	12.0	+13	+30
7 NLOS	7.2	6.9	7.4	−4.2	+2.8
Average	8.7	9.3	9.8	6.9	12.6

reduction of the delay spread. This general analysis is corroborated by the DS assessment in Tables 6 and 7, where the extension of the RT prediction to diffuse scattering actually reduces the DS value in 12 cases out of 15, and also by the following Fig. 8, where the simulated power delay profiles (PDPs) with and without scattering are shown for the TX2-RX4 case as a reference.

The highest peaks are shared by both the PDPs and correspond to the specular multipath components (i.e., reflections), whereas diffuse scattering clearly "fills the holes" between the specular contributions (since it has not to comply with strict geometrical constraints). Although the intensity of the diffused components undergo some fluctuations along the profile, the most delayed ones are clearly the weakest (at least 30 dB lower than the highest peaks) and, therefore, can be neglected in practice. Conversely, the most powerful scattered contributions occur at quite short delay, and actually belong to the head of the PDP in line with the previous, general conclusion that in-room scattering should be expected to reduce the delay spread.

In agreement with the previous considerations, Fig. 9 shows that DS decreases for increasing values of the backward scattering coefficient of the office walls. Furthermore, $S_R = 0.5$ (corresponding to a 25% of backscattered power) represents, overall, a realistic estimate for the considered scenario. This value is greater than the scattering coefficients values adopted in previous studies carried out at frequency below 6 GHz [16, 26].

Table 7 DS errors TX2

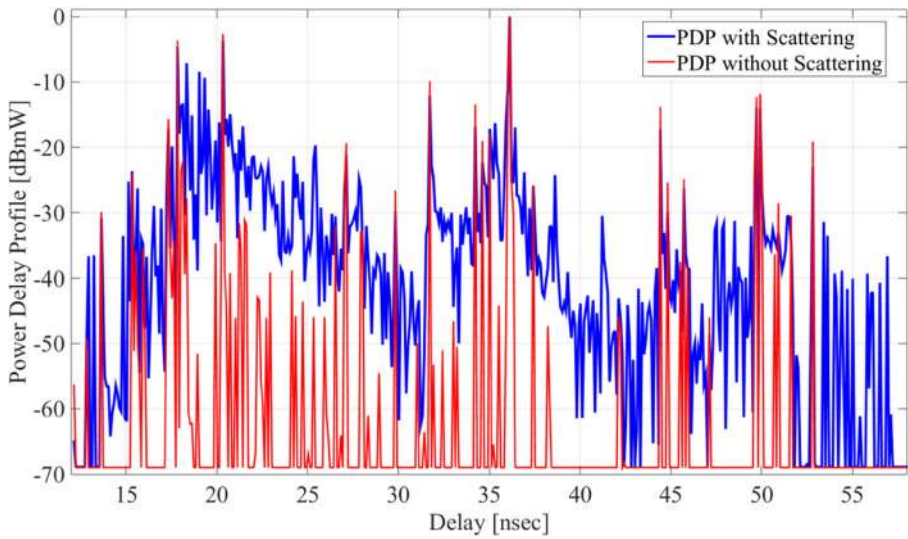| TX2	Meas. DS (nsec)	Predicted DS (nsec)		Relative DS Error %	
RXs		With scat.	Without scat.	With scat.	Without scat.
1	8.5	8.1	7.9	−5	−7
2	8.7	7.4	9.1	−15	+5
3	8.9	8.7	10.0	−2	+12
4 LOS	8.6	10.5	11.7	+22	+36
4 NLOS	8.9	9.2	9.7	+3	+9
5	9.2	8.6	10.4	−7	+13
6	8.9	8.1	8.7	−9	−2
7	7.4	10.1	9.3	+37	+26
Average	8.6	8.8	9.6	2.3	11.6

Fig. 8 Predicted PDP with and without scattering (TX2-RX4, LOS)

In conclusion, diffuse scattering due to wall irregularities at 70 GHz seems slightly stronger than at sub-6GHz frequencies in absolute terms, but it nevertheless represents a relatively minor interaction mechanism for in-room propagation.

4.4 Analysis of Propagation Mechanisms

According to the previous analysis (Table 3), in-room multipath propagation is dominated by reflections, with scattering acting as a secondary but not negligible propagation mechanism.
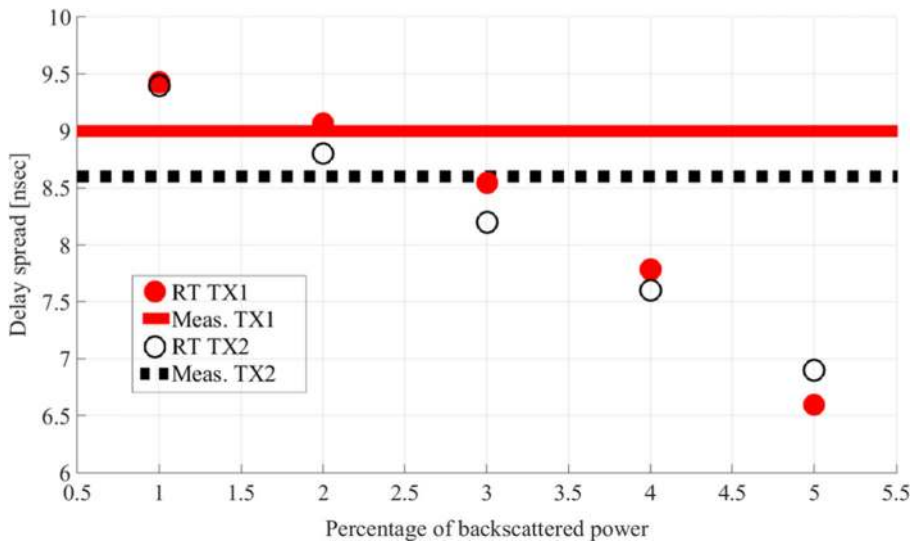

Fig. 9 Delay spread values vs. percentage of backscatter power. The *horizontal lines* correspond to the measured values whereas the *filled circles* are the RT predictions for the two TX locations

These aspects are further investigated in Fig. 10, where the contribution to the received power is separately computed through RT simulation for each interaction mechanism and for their combinations (e.g., SR corresponds to the power carried by rays experiencing both reflection and scattering). The power values for the different mechanisms have been computed for each TX-RX pair, and have been then averaged over the RX locations in order to achieve a comprehensive evaluation for each TX.

Absolute power values are reported on the vertical axis to allow some direct comparison between the TXs, whereas the corresponding relative percentage values are shown alongside the stacked bars. It is worth noticing that the percentages are related to the overall received power from the rays undergoing at least one bounce, i.e., excluding the direct path. In the following this is referred to as "NLOS received power," since it somehow represents the power that would be received if the LOS path were obstructed.

Figure 10 clearly confirms that reflection represents the dominant propagation interaction, since it contributes to convey the majority of the NLOS received power (~80 and ~70% for TX1 and TX2, respectively). Instead, diffuse scattering is responsible for an amount of NLOS power approximately ranging from 20% (TX1) to 30% (TX2).

The ratio between reflection and diffuse scattering is essentially in line with a similar analysis carried out in [20], where at least 80% of the received power has been attributed to specular interactions. The use of antennas placed at the same heights can contribute to explain the slightly larger relative amount of reflected power found in [20], since in that case the stronger reflections are expected to occur in the horizontal plane. This is not true in the present work, since the reflected paths reach the RXs with higher elevation angles due to the difference in the antennas heights, and therefore experience a lower gain of the receiving antenna.

Diffraction seems fundamentally negligible in the propagation process, in agreement with the conclusions drawn in [36].

Rays experiencing transmission only are not present due to configuration of the RX locations, being some of them in LOS condition with the TXs, and some others obstructed by the absorber, which is assumed non-penetrable due to the very high transmission loss. If combined with reflection or scattering, transmission contributes to nearly the 15 and the 25%
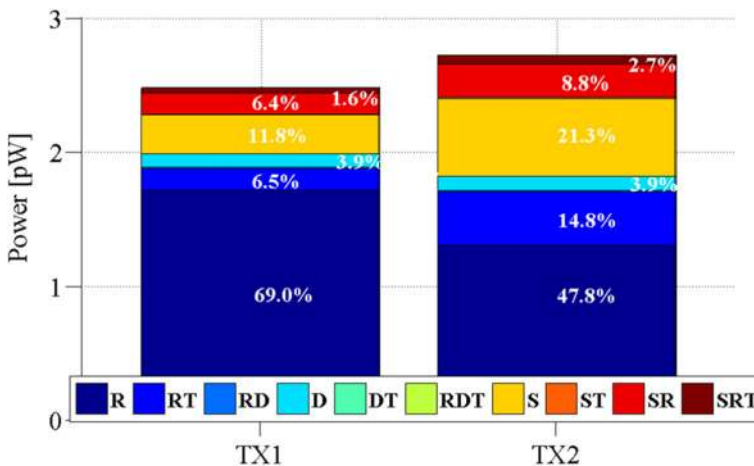

Fig. 10 Contribution of the different propagation mechanisms to the in-room received power: analysis based on RT simulation results

of the NLOS power, for TX1 and TX2, respectively. This higher than expected vale is due to transmission through tables and cupboards which have a low thickness and are made of wood or fibreboard.

Looking at the absolute power values, the scattered power received from TX2 is twice as much than the one from TX1. This is probably due to TX2 position, which is able to illuminate through scattering three out of four lateral walls (top, bottom and right side in Fig. 1), whereas TX1 only illuminates two of them (top and right side). At the same time, TX1 propagates to the RXs a much larger reflected power than TX2 (69% vs. ~48% in Fig. 10). As already noticed, this is probably due to the different inclination of the reflected paths to the RXs for TX1 and TX2. In conclusion, moving the TX towards the room corner seems to reduce scattering with respect to reflection.

5 RT Sensitivity to the Environment Description

In addition to the environment database considered so far, which includes main walls and major pieces of furniture such as windows, tables and big metal pipes (referred to as "Furnished" in the following), a more detailed representation of the small office ("detailed" in the following) also including minor pieces of furniture such as computer monitors, the blackboard, some shelves, has been considered to sound the corresponding impact on RT simulation results. Computer monitors and shelves have been modeled as dielectric slabs according to the results found in [18].

The longer computation time required by the detailed representation of the environment does not pay off in terms of better performance, especially for DS prediction, as shown in Table 8.

A possible explanation to this surprising result can be found considering that the smaller objects were measured and inserted into the database with the same manual procedure used for bigger objects, and therefore errors in the shape and position of them are relatively greater compared to their smaller size. Besides, the material composition and the corresponding electromagnetic properties of small objects such as computer monitors are less well known than those of walls, tables, and doors.

Moreover, clutter backscattering is already taken into account by the ER diffuse scattering model even in the less detailed description.

Albeit with several differences in the considered approach, the preliminary analysis sketched here is in agreement with what found in [37], where a looser point-cloud description of an indoor environment yields nearly the same prediction accuracy as a much more detailed point-cloud representation.

In conclusion, a description of the environment extended to smaller items does not seem to guarantee better RT accuracy, especially if the geometrical description of such objects is not

Table 8 Comparison of RT prediction performance for different accuracy in the description of the environment

		Furnished	Detailed
TX1	Received pow. RMSE [dB]	2.8	3.2
	PAP WRMSE [dB]	3.6	3.4
	Relative DS Error (%)	6.9	19.9
TX2	Received pow. RMSE [dB]	0.7	2
	PAP WRMSE [dB]	2.7	3.5
	Relative DS Error (%)	2.3	17.4
RT simulation time [min]		150	180

very precise and the scattering/electromagnetic properties of such small objects are largely unknown. This topic however deserves to be addressed more thoroughly in future work.

6 Conclusion

The narrowband and wideband characteristics of in-room, 70-GHz propagation are studied in this work using directional measurement and RT simulation.

The 70-GHz wireless channel appears to be dominated by a few strong contributions, with a dense multipath background distributed in time and space around them.

Although RT simulations inputs have not been accurately calibrated, a good RT prediction accuracy level has been achieved, with a total received power RMSE lower than 2 dB, a power angle profile "Weighted" RMSE of about 3 dB and a RMS delay spread percentage error of about 5%.

The RT tool has been then exploited to investigate the role played by the different interaction mechanisms within the 70 GHz wireless channel. In particular, reflections contribute with more than the 70% of the NLOS received-power, whereas diffuse scattering combined with other interactions contributes with about 20–30% of the NLOS power. In agreement with the existing literature, reflection seems to be the dominant propagation mechanism; at the same time, scattering is not negligible and seems even slightly greater than at frequencies below 6 GHz.

Most of the strong multipath contributions come from the "macro-structure" of the office; interactions with smaller furnishings elements or structural details are important in some cases, especially if made of metal.

Finally, a more detailed environment description, if subject to the same sources of error as a less detailed one, increases the computation time but does not yield a better simulations accuracy. This topic will be addressed in more detail in future work.

References

1. "Studies on frequency-related matters for International Mobile Telecommunications identification including possible additional allocations to the mobile services on a primary basis in portion(s) of the frequency range between 24.25 and 86 GHz for the future development of International Mobile Telecommunications for 2020 and beyond", Resolution 238, World Radiocommunication Conference (WRC-15), Geneve (CH), 2–27 Nov. 2015;
2. G. McCartney, T.S. Rappaport, S. Sun, S. Deng,, "Indoor Office Wideband Millimetre-Wave Propagation Measurements and Channel Models at 28 and 73 GHz for Ultra-Dense 5G Wireless Networks", IEEE Access, Vol.3, pp. 2388–2424, Dec. 2015;
3. IEEE 802.11ad International Standard for Information technology–Telecommunications and information exchange between systems-Local and metropolitan area networks–Specific requirements-Part 11: Wireless LAN Medium Access Control (MAC) and Physical Layer (PHY) Specifications Amendment 3: Enhancements for Very High Throughput in the 60 GHz Band, March 2014. http://www.ieee802.org/11/;
4. S.K. Saha, A. Garg, D. Koutsonikolas, "A first look at TCP performance in indoor IEEE 802.11ad WLANs", IEEE Conf. on Computer Communications Workshops (INFOCOM WKSHPS), Hong Kong, pp. 63–64, Apr. 26 – 1 May 2015;
5. T. S. Rappaport, S. Sun, R. Mayzus, H. Zhao, Y. Azar, K. Wang, G. N. Wong, J. K. Schulz, M. Samimi, and F. Gutierrez, "Millimeter wave mobile communications for 5G cellular: It will work!", IEEE Access, Vol. 1, pp. 335–349, May 2013;

6. C. Dehos, J.L. Gonzalez, A. De Domenico, D. Ktenas, L. Dussopt, "Millimeter-Wave Access and Backhauling: The Solution to the Exponential Data Traffic Increase in 5G Mobile Communications Systems?", IEEE Comm. Magazine, vol. 52, No. 9, pp. 88–95, Sep. 2014;

7. W. Roh et al., "Millimeter-wave beamforming as an enabling technology for 5G cellular communications: Theoretical feasibility and prototype results", IEEE Communication Magazine, vol. 52, no. 2, pp. 106–113, Feb. 2014;

8. T.E. Bogale, L.B. Le, "Massive MIMO and mmWave for 5G Wireless HetNet: Potential Benefits and Challenges", IEEE Vehicle Technology Magazine, Vol.:11, No. 1, pp. 64–75, Feb. 2016;

9. W. Fan, I. Carton, J. Nielsen, K. Olesen, G.F. Pedersen, "Measured wideband characteristics of indoor channels at centimetric and millimetric bands", Eurasip Journal on Wireless Communications and Networking, Feb. 2016;

10. D. Dupleich, F. Fuschini, R. Müller, E. M. Vitucci, C. Schneider, V. Degli-Esposti, and R. S. Thomä, "Directional characterization of the 60 GHz indoor-office channel", XXXIth URSI General Assembly and Scientific Symposium, Beijing, 16–23 Aug. 2014, pp. 1–4;

11. F. Fuschini, E. M. Vitucci, M. Barbiroli, G. Falciasecca, V. Degli-Esposti, "Ray tracing propagation modeling for future small-cell and indoor applications: A review of current techniques", Radio Science, vol. 50, No. 6, pp. 469–485, Jun. 2015;

12. S. Hur, S. Baek, B. Kim, Y. Chang, A.F. Molisch, T.S. Rappaport, K. Haneda, J. Park, "Proposal on Millimeter-Wave Channel Modeling for 5G Cellular System", IEEE Journal on Selected Topics in Signal Processing, vol. 10, No. 3, pp. 454–469, Apr. 2016;

13. N. Zhang; L. Tian, X. Yuan, X. Yang, S. Mei, H. Wang, "Dynamic Channel Modeling for an Indoor Scenario at 23.5 GHz", IEEE Access, vol. 3, pp. 2950–2958, Dec. 2015;

14. Y. Corre, T. Thenoux, J. Stephan, F. Letourneoux, Y. Lostanlen, "Analysis of Outdoor Propagation and Multi-Cell Coverage from Ray-Based Simulations in sub-6GHz and mmWave Bands", in 10th Eur. Conf. Antennas and Propagation (EuCAP2016), Davos (CH), pp.1-5. 2016;

15. A. Navarro Cavidad, D. Guevara Ibarra, S. Londono Salcedo "Using 3-D Video Game Technology in Channel Modeling", IEEE Access, vol. 2, pp. 1652–1659, Jan. 2015;

16. F. Mani, F. Quitin, C. Oestges, "Directional Spreads of Dense Multipath Components in Indoor Environments: Experimental Validation of a Ray-Tracing Approach", IEEE Transactions on Antenna and Propagation, vol. 60, No. 7, pp. 3389–3396, Jul. 2012;

17. P. Pongsilamanee, H. L. Bertoni, "Specular and nonspecular scattering from building facades", IEEE Transactions on Antenna and Propagation, vol. 52, No. 7, pp. 1879–1889, Jul. 2004;

18. F. Fuschini, S. Häfner, M. Zoli, R. Müller, E. M. Vitucci, D. Dupleich, M. Barbiroli, J. Luo, E. Schulz, V. Degli-Esposti, R.S. Thomä, "Item level characterization of mm-wave indoor propagation", Eurasip Journal on Wireless Communications and Networking, Feb. 2016;

19. K. Haneda, "Channel models and beamforming at millimeter-wave frequency bands", IEICE Trans on Communications vol. E98B, No. 5, pp. 755–772, May 2015;

20. K. Haneda, J. Järveläinen, A. Karttunen, M. Kyro, J. Putkonen, "A Statistical Spatio-Temporal Radio Channel Model for Large Indoor Environments at 60 and 70 GHz", IEEE Trans. on Ant. and Propagat. vol. 63, No. 6, pp. 2694–2704, Jun. 2015;

21. J. Järveläinen, K. Haneda, "Sixty gigahertz indoor radio wave propagation prediction method based on full scattering model", Radio Science, vol. 49, No. 4, pp. 293–305, Apr. 2014;

22. D. A. Dupleich, S. Häfner, C. Schneider, R. Müller and R. S. Thomä, "Double-Directional and Dual-Polarimetric Indoor Measurements at 70 GHz", IEEE 26th International Symposium on Personal, Indoor and Mobile Radio Communications (PIMRC 2015): Workshop on 5G Channel Measurement and Modeling, Hong Kong, Aug. 30 – Sep. 2, 2015;

23. S. Häfner, D. A. Dupleich, R. Müller, C. Schneider and R. S. Thomä, "Characterisation of Channel Measurements at 70GHz in Indoor Femtocells", IEEE 81st Veh. Tech. Conf., Glasgow (UK), pp 1–5, 11–14 May, 2015;

24. S. Häfner, D. A. Dupleich, R. Müller, C. Schneider and R. S. Thomä, "Ultra-Wideband Channel Sounder for Measurements at 70 GHz", IEEE 81st Veh.Tech.Conf., Glasgow (UK), pp. 1–5, 11–14 May 2015;

25. V. Degli-Esposti, F. Fuschini, E. M. Vitucci, G. Falciasecca, "Measurement and modelling of scattering from building", IEEE Transactions on Antenna and Propagation,Vol.55 no.1, pp.143–153, Jan. 2007;

26. F. Fuschini, V. Degli-Esposti, E. M. Vitucci, "A model for forward-diffuse scattering through a wall", 4th Eur. Conf. Antennas and Propagation (EuCAP 2012), Barcelona (SP), pp. 1–4, 2010;

27. I. Cuinas, J.-P. Pugliese, A. Hammoudeh, M.G. Sanchez, "Comparison of the electromagnetic properties of building materials at 5.8 GHz and 62.4 GHz", 52nd Vehicle Technology Conf., Boston (MA), pp. 780–785, 2000;

28. D. Ferreira, I. Cuinas, R.F.S. Caldeirinha, T.R. Fernandes, "A review on the electromagnetic characterization of building materials at micro- and millimetre wave frequencies", 8th Eur. Conf. Antennas and Propagation (EuCAP2014) The Hague (NL), pp. 145–149, 6–11 Apr. 2014;

29. J. Lu, D. Steinbach, P. Cabrol, P. Pietraski, R.V. Pragada, "Propagation characterization of an office building in the 60 GHz band", 8th Eur. Conf. Antennas and Propagation (EuCAP 2014), The Hague (NL), pp. 809–813, 2014;

30. J. Pascual-García, J. M. Molina-García-Pardo, M. T. Martínez-Inglés, J. V. Rodríguez, N. Saurín-Serrano, "On the Importance of Diffuse Scattering Model Parameterization in Indoor Wireless Channels at mm-Wave Frequencies", Vol:4, pp: 688–701, IEEE Access, Feb 2016;

31. M. Peter, W. Keusgen, R. Felbecker, "Measurement and Ray-Tracing Simulation of the 60 GHz Indoor Broadband Channel: Model Accuracy and Parameterization", 2nd Eur. Conf. Antennas Propag. (EuCAP 2007) Edinburgh, UK, pp. 1–8, 11–16 Nov. 2007;

32. E. M. Vitucci, F. Fuschini, V. Degli-Esposti, "Ray Tracing simulation of the radio channel time-and angle-dispersion in large indoor environments", 8th Eur. Conf. Antennas and Propagation (EuCAP 2014), The Hague (NL), pp. 1771–1774, 6–11 Apr. 2014;

33. F. Mani, C. Oestges, "Ray-tracing evaluation of diffuse scattering in outdoor scenario", 5th Eur. Conf. Antennas and Propagation (EuCAP 2011), Rome (IT), pp. 3439–3443,11-15 Apr. 2015;

34. F. Fuschini, H. El-Sallabi, V. Degli-Esposti, L. Vuokko, D. Guiducci, P. Vainikainen, "Analysis of multipath propagation in urban environment through multidimensional measurements and advanced ray tracing simulation", IEEE Transaction on Antennas and Propagation, Vol.56 no.3, pp. 848–857, Mar. 2008;

35. V. Degli-Esposti, F. Fuschini, E. M. Vitucci, "A fast model for distributed scattering from buildings", 3rd European Conference on Antennas and Propagation (EuCAP 2009), Berlin, Germany, 23–27 March 2009.

36. M. Jacob, S. Priebe, R. Dickhoff, T. Klein-Ostmann, T. Schrader, T. Kürner, "Diffraction in mm and Sub-mm Wave Indoor Propagation Channels", IEEE Trans. on Microwave Theory and Tech., vol. 60, No. 3 pp. 833–844, Mar. 2012;

37. J. Järveläinen, M. Kurkela, K. Haneda, "Impacts of Room Structure Models on the Accuracy of 60 GHz Indoor Radio Propagation Prediction", IEEE Antennas and Propagat. Letters, vol. 14, no.3, pp. 1137–1140, Jan. 2015